DOI: 10.1002/cbic.200800318

Direct Epoxidation in *Candida antarctica* Lipase B Studied by Experiment and Theory

Maria Svedendahl,[a] Peter Carlqvist,[b, c] Cecilia Branneby,[a, d] Olof Allnér,[b, e] Anton Frise,[b] Karl Hult,[a] Per Berglund,*[a] and Tore Brinck*[b]

Candida antarctica *lipase B (CALB) is a promiscuous serine hydrolase that, besides its native function, catalyzes different side reactions, such as direct epoxidation. A single-point mutant of CALB demonstrated a direct epoxidation reaction mechanism for the epoxidation of α,β-unsaturated aldehydes by hydrogen peroxide in aqueous and organic solution. Mutation of the catalytically active Ser105 to alanine made the previously assumed indirect epoxidation reaction mechanism impossible. Gibbs free energies, activation parameters, and substrate selectivities were determined both computationally and experimentally. The energetics and mechanism for the direct epoxidation in CALB Ser105Ala were investigated by density functional theory calculations, and it was demonstrated that the reaction proceeds through a two step-mechanism with formation of an oxyanionic intermediate. The active-site residue His224 functions as a general acid-base catalyst with support from Asp187. Oxyanion stabilization is facilitated by two hydrogen bonds from Thr40.*

Introduction

The epoxide functional group is one of the most useful intermediates in organic synthesis, since it easily undergoes stereospecific ring-opening to form bifunctional compounds. Epoxidation of an unsaturated compound can be affected by hydrogen peroxide or molecular oxygen. Hydrogen peroxide is a preferred oxidant from an environmental perspective, since the reaction can be carried out in aqueous media and gives only water as by-product. It is also favorable for industrial production of epoxides, due to its low cost and availability in bulk quantities. However, the epoxidation of unsaturated compounds with hydrogen peroxide is usually slow and needs the addition of a catalyst. Examples of available catalysts include silica-supported titanium,[1] methyltrioxorhenium,[2,3] iron complexes,[4,5] and manganese(II) salts.[6]

In industrial catalysis there is increasing interest in the use of enzyme and peptide catalysts to fulfill the requirement for stereoselective catalysis without the need for toxic and expensive transition metal catalysts. There are several enzymes that catalyze epoxidations. Haloperoxidases[7–10] constitute an enzyme family that catalyzes epoxidation of alkenes. Chloroperoxidase is a member of this family and catalyzes the stereoselective epoxidation of alkenes with good yields. Lipases[11–16] have been used for the indirect epoxidation of alkenes with hydrogen peroxide through the formation of peroxy acids. The actual epoxidation of the alkene takes place outside the enzyme. The indirect reaction mechanism of *Candida antarctica* lipase B (CALB) begins with the formation of an acylenzyme through the binding of Ser105 to the carbonyl carbon of a carboxylic acid. Hydrogen peroxide then attacks the carbonyl carbon to form a carboxylic peracid, which departs from the active site. The carboxylic peracid reacts with an alkene outside the enzyme to form the final epoxide. The produced epoxides showed no stereoselectivity. Monooxygenases,[17,18] such as cytochrome P-450, activate molecular oxygen and incorporate one oxygen atom into the substrate and reduce the other atom to water. The main drawback with these enzymes is that they are dependent on a cofactor and require NADPH recycling, which in preparative chemistry can be achieved by the use of microbial cells. Unfortunately, the cells are sensitive and suffer degradation by the formed epoxide. Polyamino acids,[19] such as polyleucine, behave as synthetic enzymes and catalyze the epoxidation of unsaturated ketones with hydrogen peroxide.

Here we present a new promiscuous reaction catalyzed by CALB: the direct epoxidation of α,β-unsaturated aldehydes with hydrogen peroxide. CALB catalyzes epoxidation reactions by activating both hydrogen peroxide and an α,β-unsaturated aldehyde and bringing them into suitable positions for reaction. Mutation of the nucleophilic Ser105 to the nonpolar ala-

[a] *M. Svedendahl, Dr. C. Branneby, Prof. K. Hult, Prof. P. Berglund*
Department of Biochemistry, Royal Institute of Technology (KTH)
AlbaNova University Center, 106 91 Stockholm (Sweden)
Fax: (+46) 8-5537-8483
E-mail: per.berglund@biotech.kth.se

[b] *Dr. P. Carlqvist, O. Allnér, A. Frise, Prof. T. Brinck*
Physical Chemistry, Royal Institute of Technology (KTH)
100 44 Stockholm (Sweden)
Fax: (+46) 8-790-8207
E-mail: tore@physchem.kth.se

[c] *Dr. P. Carlqvist*
Present address: Medivir AB, P.O. Box 1086
SE-14 122 Huddinge (Sweden)

[d] *Dr. C. Branneby*
Present address: BASF Aktiengesellschaft, Abt. GVF/E-A 30
67056 Ludwigshafen (Germany)

[e] *O. Allnér*
Present address: Centre for Structural Biochemistry
Karolinska Institute, 14 157 Huddinge (Sweden)

nine leaves His224 to act as a base directly towards hydrogen peroxide. The reaction cannot proceed by the indirect epoxidation mechanism, since the mutant lacks the nucleophilic serine 105. The mechanism for the direct epoxidation in the mutant, CALB Ser105Ala, has been investigated by molecular dynamics simulations and density functional theory calculations. It is suggested that the reaction proceeds via an oxyanion intermediate and that His224 functions as a general acid-base catalyst (Scheme 1).

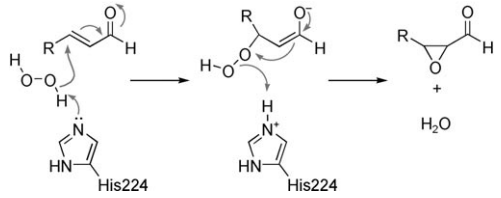

Scheme 1. Direct epoxidation of an α,β-unsaturated aldehyde with hydrogen peroxide catalyzed by CALB Ser105Ala. The residue His224 functions as a general acid-base catalyst.

C. antarctica lipase B (CALB) is a serine hydrolase. The catalytic function of native CALB is well understood, as are the roles of the different amino acids in the active site. The catalytically important active-site amino acids are Asp187, His224, Ser105, Gln106, and Thr40. The histidine, together with the aspartate and serine, constitute what is known as the catalytic triad. The glutamine and threonine form the oxyanion hole, a hydrogen bonding network that stabilizes negatively charged oxyanion intermediates.[20] CALB has well-known promiscuous behavior, and its active site have been used as a scaffold to perform types of reactions other than its native hydrolysis of esters.[21,22] We have previously studied CALB, both computationally and experimentally, for the Baeyer–Villiger oxidation,[23] aldol addition,[24,25] and conjugate addition.[26,27] In this paper we demonstrate a new promiscuous reaction of CALB: direct epoxidation.

Results and Discussion

The direct epoxidation reaction

CALB was used to demonstrate direct epoxidation of α,β-unsaturated aldehydes with hydrogen peroxide. This CALB-catalyzed direct epoxidation was studied both experimentally and computationally. In the experimental study, the epoxidation of but-2-enal (0.3 M) with hydrogen peroxide (0.4 M) was chosen as a type reaction. Immobilized wild-type CALB and CALB Ser105Ala were compared in this reaction both in buffer (100 mM KH_2PO_4, pH 3.9) and in organic solution (acetonitrile). The pH of the reaction buffer was chosen to avoid decomposition of the hydrogen peroxide, although the optimal pH for the enzyme would be over the pK_a value of His224 in CALB. It should also be noted that the His224 will be protonated in water.

The lack of epoxidation product when active-site-inhibited CALB was used demonstrated that the reaction took place in the active site. Furthermore, both the active-site mutant CALB Ser105Ala and the wild-type enzyme catalyzed the reaction; this shows that no acyl enzyme intermediate leading to a peroxy acid was involved.

The yield in acetonitrile was 80% with but-2-enal and CALB Ser105Ala as catalyst after 17.5 days, whereas only a 44% yield was reached for the same reaction and time with wild-type CALB. Yields were estimated from the GC analysis and are not isolated yields.

Enzyme kinetics

Enzyme kinetics for wild-type CALB and CALB Ser105Ala were examined both in buffer and in acetonitrile (Table 1). A series of direct epoxidation reactions were followed under pseudo-one-substrate conditions, the concentration of hydrogen peroxide was constant at 0.4 M, while the concentration of the oxyanion binding substrate (aldehyde) was varied. The following kinetic constants are apparent, since only one substrate was varied. The apparent specificity constant (k_{cat}^{app}/K_M^{app}), the apparent Michaelis constant K_M^{app}, and the apparent turnover number k_{cat}^{app}, were calculated for wild-type CALB and for CALB Ser105Ala. No saturation was found in acetonitrile at substrate concentrations up to 3 M. An increase in catalytic proficiency was achieved in acetonitrile relative to buffer. The increase could be attributed to a lower k_{non} value expressed in acetonitrile than in buffer solution. Direct epoxidation of 3-phenylprop-2-enal with hydrogen peroxide was only performed in acetonitrile, and the (k_{cat}^{app}/K_M^{app}) was much lower than for but-2-

Table 1. Apparent kinetic constants calculated for the direct epoxidation of two α,β-unsaturated aldehydes by hydrogen peroxide (0.4 M) under pseudo-one-substrate conditions in buffer or acetonitrile, catalyzed by wild-type CALB and by Ser105Ala at 20 °C.

Enzyme	k_{cat}^{app} [min^{-1}]	K_M^{app} [M^{-1}]	k_{cat}^{app}/K_M^{app} [$M^{-1}min^{-1}$]	k_{non} [$M^{-1}min^{-1}$]	$\frac{k_{cat}^{app}}{K_M^{app}}/k_{non}$
wild-type CALB					
but-2-enal					
in buffer	22	0.24	94	3×10^{-5}	3×10^{6}
in acetonitrile	n.s.[a]	n.s.[a]	6	6×10^{-7}	1×10^{7}
3-phenylprop-2-enal					
in acetonitrile			0.003	2×10^{-7}	2×10^{5}
CALB Ser105Ala					
but-2-enal					
in buffer	34	0.19	180	3×10^{-5}	6×10^{6}
in acetonitrile	n.s.[a]	n.s.[a]	9	6×10^{-7}	2×10^{7}
3-phenylprop-2-enal					
in acetonitrile			0.03	2×10^{-7}	2×10^{6}

[a] n.s. = no saturation was reached at aldehyde concentrations up to 3 M.

enal for both CALB variants. The enzymes were not found to introduce any stereoselectivity in the epoxidation reactions and only racemic products were obtained.

Experimentally determined Gibbs free energy of activation

The Gibbs free energies of activation for the direct epoxidation of but-2-enal with hydrogen peroxide were determined experimentally both for wild-type CALB and for CALB Ser105Ala in KH_2PO_4 buffer solution (100 mM, pH 3.9) and acetonitrile. The enzyme kinetic study (Table 1) resulted in the Gibbs free energy changes presented in Table 2. A temperature study, in which the direct epoxidation reactions were performed at different temperatures, gave the activation parameters shown in Table 3. The Gibbs free energies of activation ($\Delta G^{\ddagger}$) from the temperature study agreed well with the corresponding energies from the kinetic study. $\Delta\Delta G$ shows the enzyme contribution, the difference between enzyme-catalyzed reactions and background reactions. These values are near 40 kJ mol^{-1}. Magnusson et al. showed by a comparison of wild-type CALB and a Thr40Ala mutant that the value of one hydrogen bond is 20 kJ mol^{-1}.[28] From this knowledge it can be deduced that two hydrogen bonds were formed in the transition state.

The $\Delta\Delta G$ value for the epoxidation reaction can also be compared to the $\Delta\Delta G$ value for the conjugate addition reaction performed by the same CALB mutant. In that case, 2.2 to 2.5 hydrogen bonds were formed, depending on the substrates.[26,27] The Gibbs free energies of activation ($\Delta G^{\ddagger}$), enthalpies of activation ($\Delta H^{\ddagger}$), and entropies of activation ($\Delta S^{\ddagger}$) were similar for both CALB variants. The reaction in acetonitrile has a more negative activation entropy than the reaction in buffer both for the wild type and for the mutant. This can be attributed to the larger entropy gain from desolvation of the substrate in the buffer. The uncatalyzed epoxide reaction in buffer solution differed from the enzyme-catalyzed reactions in a much larger entropy contribution to the activation free energy. In this case, the difference is probably due to the need to reorganize the water molecules to stabilize the transition state in the buffer reaction.

Table 2. Experimentally determined Gibbs free energy calculated from the results in Table 1.

Enzyme	ΔG_{ES}[b] [kJ mol^{-1}]	$\Delta G_{ES}^{\ddagger}$[b] [kJ mol^{-1}]	$\Delta G_{k_{cat}}$[b] [kJ mol^{-1}]	$\Delta G_{k_{non}}$[b] [kJ mol^{-1}]	$\Delta\Delta G$[b] [kJ mol^{-1}]
wild-type CALB					
but-2-enal[a]					
in buffer	−4	72	75	109	−37
in acetonitrile		79		119	−40
CALB Ser105Ala					
but-2-enal[a]					
in buffer	−4	70	74	109	−39
in acetonitrile		78		113	−41

[a] Reaction conditions: 0.3 M aldehyde, 0.4 M hydrogen peroxide, 0.3 M 1,4-dioxane or decane as internal standard, solvent (100 mM KH_2PO_4 buffer of pH 3.9 or acetonitrile) was added to a total volume of 750 μL and 12.5 mg immobilized enzyme. [b] Calculated for 298 K.

Molecular dynamics simulations

Molecular dynamics (MD) simulations performed with the Ser105Ala mutant and the substrate molecules—hydrogen peroxide and 3-phenylprop-2-enal—in the active site provide information on the substrate binding and on how well the dynamic properties of the enzyme promote the reaction. The simulations are analyzed with respect to a number of interatomic distances relevant to the catalytic process (Figure 1). The focus is on the results of the simulations in water, but the acetonitrile simulations are included for comparison. As can be seen in Table 4, the hydrogen peroxide stays tightly bound to His224 through a hydrogen bond for most of the simulation time. In acetonitrile solution, the distance between the histi-

Table 3. Experimentally determined activation parameters for the direct epoxidation[a] of but-2-enal with hydrogen peroxide catalyzed by wild-type CALB and CALB Ser105Ala in buffer and in acetonitrile.

Enzyme	$\Delta G^{\ddagger}$[b] [kJ mol^{-1}]	$\Delta H^{\ddagger}$ [kJ mol^{-1}]	$\Delta S^{\ddagger}$[b] [J mol^{-1} K]
wild-type CALB			
in buffer	78	65	−45
in acetonitrile	82	58	−81
CALB Ser105Ala			
in buffer	76	63	−43
in acetonitrile	80	61	−64
uncatalyzed			
in buffer	109	69	−134

[a] Reaction conditions: 0.3 M aldehyde, 0.4 M hydrogen peroxide, 0.3 M 1,4-dioxane or decane as internal standard, solvent (100 mM KH_2PO_4 buffer of pH 3.9 or acetonitrile) was added to a total volume of 750 μL and 12.5 mg immobilized enzyme. [b] Calculated for 298 K.

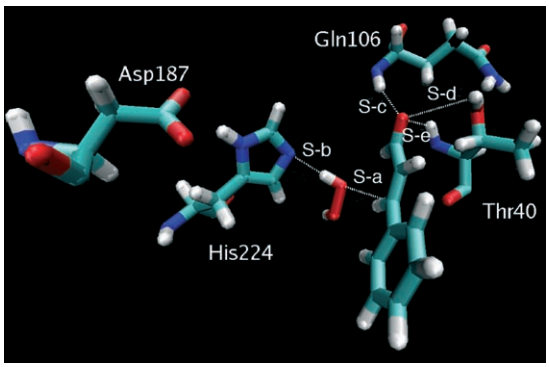

Figure 1. A snapshot from MD simulations of the positions of the reactants in the active site of Ser105Ala mutant in the epoxidation of 3-phenylprop-2-enal. Only the catalytically important residues are depicted. White broken lines mark the catalytically important distances that were analyzed.

Table 4. Analysis of catalytically important distances from the MD simulations on substrate binding of 3-phenylprop-2-enal in the Ser105Ala mutant. Fraction (*P*) of distance values within the sum of van der Waals radii and average distances are given.

Solvent distances[a]	Water		Acetonitrile	
	P[b]	average [Å]	*P*[a]	average [Å]
S-a	0.000	4.9	0.032	3.7
S-b	0.609	2.2	0.619	2.3
S-c	0.145	2.3	0.005	2.9
S-d	0.001	3.3	0.000	3.4
S-e	0.149	2.4	0.064	2.5

[a] For definition of distances see Figure 1. [b] The reference value for the –C···O distance (**S-a**) is 3.1 Å and that for the hydrogen bonds (**S-b**···**S-e**) is 2.0 Å. Reference values are based on van der Waals radii taken from reference,[29] and for the hydrogen bonds the repulsive potential is assumed to come from the nonhydrogen atoms.

dine nitrogen and hydrogen peroxide hydrogen (**S-b**) stays within 2.0 Å for 62% of the simulation time, and the average distance is 2.3 Å. The results in aqueous solution are very similar. The simulations thus indicate that substrate binding of hydrogen peroxide is not a limiting factor for catalysis if the hydrogen peroxide concentration is sufficient. The binding of 3-phenylprop-2-enal is analyzed with respect to the ability to form hydrogen bonds with the oxyanion hole. Here the interest lies in the distances between the oxygen and the backbone N–H hydrogens of residues Gln106 and Thr40, and the distance between the oxygen and the O–H hydrogen of Thr40. Interestingly, we find that the 3-phenylprop-2-enal is not strongly hydrogen-bonded to the oxyanion hole. The hydrogen bond to the Thr40 N–H group (**S-e**) stays within a distance of 2.0 Å for only 15% of the simulation time. The average distance is as long as 2.4 Å. The hydrogen bond to Gln106 (**S-c**) is of similar importance: 14% within 2.0 Å and average distance of 2.3 Å. The Thr40 O–H group is basically rotated away from the carbonyl carbon of the substrate during the entire simulation; the average distance is 3.4 Å. Interestingly, the simulations shows that the substrate binds much more weakly to the oxyanion hole in acetonitrile than it does in aqueous solution. In acetonitrile, there is a short hydrogen bond (<2.0 Å) between the substrate and the oxyanion hole for less than 7% of the time. The average **S-c** value is increased from 2.3 Å with water solvation to 2.9 Å with acetonitrile. The relatively weaker substrate binding in acetonitrile than in water is in agreement with the kinetic study: a K_M^{app} value of 0.19 M^{-1} was determined in water, whereas saturation of the enzyme in acetonitrile was not reached even at a substrate concentration of 3 M.

Another point of interest is the ability of the substrate molecules to form near attack conformers (NACs).[30,31] These are ground state conformers in which the atoms involved in the bond making are at the van der Waals distance. In the first step of the epoxidation reaction a bond is formed between an oxygen of hydrogen peroxide and the β-carbon of the α,β-unsaturated aldehyde, in concert with the transfer of the oxygen proton to the histidine nitrogen. Thus, the NAC of the initial step has both the oxygen–carbon (**S-a**) and the hydrogen–nitrogen (**S-b**) distance within the van der Waals distance. We have already noted that the **S-b** distance is below 2.0 Å during 62% of the simulation time. However, the **S-a** distance fulfills the NAC criteria only 3.2% of the time in the acetonitrile simulation. In water the corresponding result is below 0.1%. It should be noted that the starting complex of the DFT calculations is basically a NAC. The free energy required to form the NAC (ΔG_{NAC}) is thus an approximation for the free energy of going from the initial substrate complex to the DFT starting complex, and should be added to the quantum chemical activation energy to provide an estimate of the free energy barrier for the first reaction step.[25] This barrier contribution can be estimated from Equation (1):

$$\Delta G_{NAC} = -RT \ln P \quad (1)$$

where *P* is the fraction of structure that fulfills the NAC criteria. A NAC fraction of 3.2% then corresponds to an increase in the barrier by 9 kJ mol^{-1}. It should be noted that this value is only a lower limit to the effect, since we have applied a rather loose NAC definition. A more correct NAC definition requires both the **S-a** and the **S-b** distances to be within their limits at the same time, as there are hydrogen bonds between the oxyanion hole and the carbonyl oxygen. We are not able to obtain a free energy correction with this definition, since there are too few structures that simultaneously fulfill all the criteria. However, it can be concluded that the unfavorable substrate binding may have a significant effect on the kinetics of the reaction.

The binding of the reaction intermediate to the active site is also of importance for the reactive properties. In this case the relevant distances are depicted in Figure 2. It can first be noted that the formed oxyanion binds much more strongly than the carbonyl oxygen of the substrate to the oxyanion hole. In the intermediate the hydrogen bonds to the N–H (**I-d**) and O–H (**I-c**) groups of Thr40 are both within 2.0 Å more than 90% of the simulation time (Table 5). Interestingly, we find that the N···H bond to the Gln106 is much weaker and only within hydrogen bond distance 13% of the time. The results of the acetonitrile simulation show a slightly higher frequency of

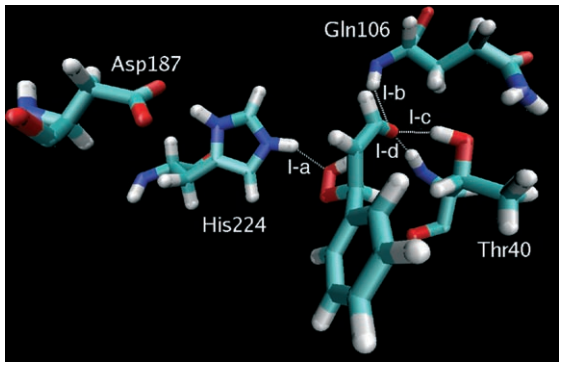

Figure 2. A snapshot from the MD simulations of the position of the reaction intermediate in the active site of Ser105Ala mutant in the 3-phenylprop-2-enal epoxidation. Only the catalytically important residues are depicted, whereas broken lines mark the catalytically important distances that were analyzed.

Table 5. Analysis of catalytically important distances from the MD simulations on reaction intermediate binding of 3-phenylprop-2-enal in the Ser105Ala mutant. Fractions (*P*) of distance values within the sum of van der Waals radii and average distances are given.

Solvent distances[a]	Water		Acetonitrile	
	P[a]	average [Å]	*P*[a]	average [Å]
I-a	0.170	4.9	0.077	2.5
I-b	0.128	2.2	0.171	2.3
I-c	0.909	2.3	0.988	1.7
I-d	0.911	3.3	0.902	1.9

[a] For definition of distances see Figure 2. [b] The reference value for the hydrogen bonds (**I-a**···**I-d**) is 2.0 Å.

hydrogen bonding to Gln106 (17%). This indicates that the Gln106 N···H system has a much smaller effect in stabilizing the intermediate than the Thr hydrogen bonds.

The frequency of NAC information in the intermediate is of importance for the kinetic properties of the second reaction step: that is, the peroxide formation. Here, the relevant parameter is the distance between the His224 hydrogen and the outer oxygen of the peroxy group (**I-a**). The percentage of NAC formation is 7.7% in acetonitrile and 17% in water. These results suggest that NAC formation in the intermediate is not a major obstacle for the reaction, and may only be of importance if the transition state energy for the second reaction step is significantly higher than for the first.

Density functional theory modeling

The DFT modeling was performed in two different model systems. The first model (model 1) includes a full representation of the oxyanion hole, whereas the second (model 2) lacks the Gln106 functionality (Figure 3). This latter model was considered because the MD simulations indicate that there is no hydrogen bond between the Gln106 N–H group and the oxyanion of the reaction intermediate, and that Gln106 therefore cannot influence the reaction. Computations were performed

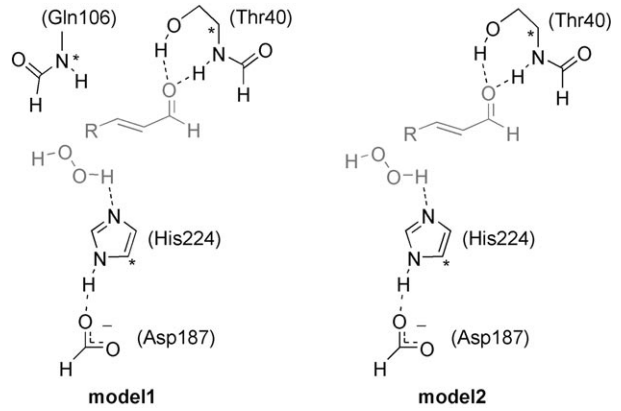

Figure 3. Model systems used in the DFT calculations, with the substrates—hydrogen peroxide and the aldehyde—in gray. Atoms marked by an asterisk were constrained.

both for but-2-enal and for 3-phenylprop-2-enal in both model systems.

The epoxidation of the unsaturated aldehyde is predicted to take place in two steps inside the active site of the mutant enzyme (Scheme 2). In the DFT model systems, the reaction

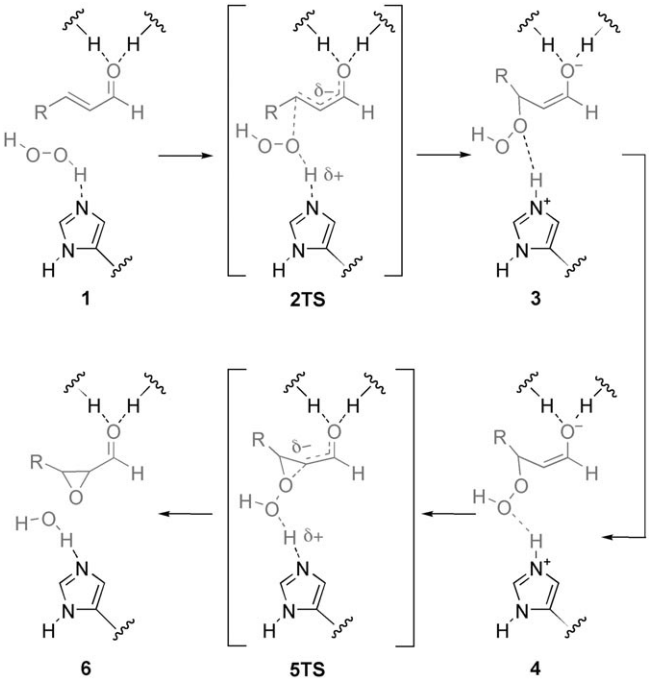

Scheme 2. The detailed reaction mechanism for the epoxidation in CALB Ser105Ala deduced from the DFT computations.

starts from a near attack complex (reaction complex), in which the unsaturated aldehyde is bonded to the oxyanion hole through hydrogen bonds to Thr40. Furthermore, there is a hydrogen bond between the Gln106 N–H group and the peroxide in the large model (model 1).

In the first step (**2TS**, Scheme 2, Figure 4) of the reaction the His224 abstracts a proton from the hydrogen peroxide, and at the same time the inner oxygen forms a bond to the β-carbon of the aldehyde. The hydrogen bond network of the oxyanion hole remains throughout this step. In the reaction with but-2-enal as substrate, this step has barriers of 49 and 33 kJ mol^{-1} (Table 6) for the reaction complexes for model 1 and model 2, respectively. This relatively low barrier is explained by two important features of the active site. 1) The hydrogen peroxide is activated by the abstraction of a proton by His224, and the resulting positive charge is stabilized by Asp187. 2) The negative charge that is formed on the aldehyde is transferred through resonance to the carbonyl oxygen, where it is stabilized by the two hydrogen bonds from Thr40.

The result of these two factors is mainly a stabilization of the charge separation in the transition state and provides an explanation for the low activation energy. The reaction intermediate **3** rearranges to **4** before the reaction proceeds; the hydrogen bond between His224 and the hydrogen peroxide switches from the inner to the outer oxygen of the hydrogen

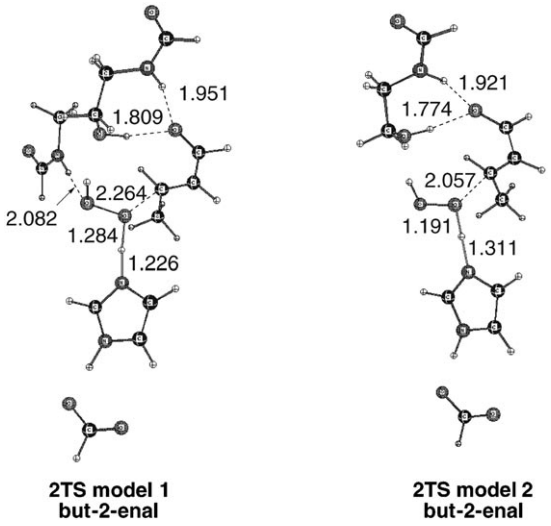

Figure 4. Transition state structures (**2TS**) for the rate-determining step of but-2-enal epoxidation for the two models.

Table 6. Relative energies [B3LYP/6-311 + G(d)] in kJ mol^{-1} for the epoxidation of but-2-enal and 3-phenylprop-2-enal in the model systems.

Substrate	$\Delta E^{[a]}$ but-2-enal		$\Delta E^{[a]}$ 3-phenylprop-2-enal	
	model 1	model 2	model 1	model 2
1	0	0	0	0
2TS	49	33	59	52
3	−1	−20	23	11
4	1	−21	24	8
5TS	30	10	54	41
6	−163	−177	−143	−144

[a] Relative energies have been corrected for solvation effects at the PCM level with use of a dielectric constant of 4.

peroxide. The energy difference between the two intermediates is small (less than 4 kJ mol^{-1}) and we were not able to locate a transition state for the transfer. The second step of the reaction is the actual formation of the epoxide **5TS**. A bond is formed between the α-carbon of the aldehyde and the inner oxygen of hydrogen peroxide, and at the same time the proton on His224 is transferred to the outer oxygen of hydrogen peroxide, forming water. Again, the hydrogen bonding network of the oxyanion hole remains unchanged. With but-2-enal as substrate in model 1, this step has a barrier of 29 kJ mol^{-1}relative to **4**, and **5TS** lies 30 kJ mol^{-1} above the reaction complex. The corresponding energy differences for model 2 are 31 and 10 kJ mol^{-1}, respectively.

The qualitative picture of the reaction sequence is similar for the two model systems. In both cases the initial proton transfer step is rate-determining, and the energetics suggest that there should be no accumulation of reaction intermediate. This is in agreement with the experimental results, which found no saturation in the kinetics with respect to the aldehyde even at 3 M in acetonitrile; accumulation of reaction intermediate will lead to saturation. Interestingly, we find no propensity for the Gln N–H group to form a hydrogen bond to the oxygen of the aldehyde during the reaction in model 1. This is not entirely surprising in view of the fact that the MD results also show that the hydrogen bond stabilization of the oxyanion in the intermediate dominantly comes from Thr40. However, in the quantum chemical simulation with model 1 there is a hydrogen bond interaction between the Gln N–H and one of the oxygens of the peroxy group that is absent in the MD simulations. The difference in behavior is most likely an effect of the lack of explicit solvent molecules and the reduced active site model in the QM calculations, which limits the interaction possibilities. A quantitative analysis shows that both the first- and second-step transition barriers are higher in model 1 than in model 2. This seems to be a consequence of the extra hydrogen bond between Gln and the peroxy group in model 1. Since this interaction seems to simulate a solvation interaction in the real system, it is not unlikely that the large system calculations are more accurate. It should also be noted that the unspecific solvation corrections from the polarizable continuum model have the effect of raising the transition barriers.

The reaction with 3-phenylprop-2-enal is found to have a reaction profile similar to that of the but-2-enal reaction in both model systems. However, the relative transition state energies are higher for 3-phenylprop-2-enal, and the biggest difference is found for the second step of the reaction. Still, also for 3-phenylprop-2-enal, the quantum chemical calculations predict the first step to be rate-determining. In the large model system (model 1) calculations, the 3-phenylprop-2-enal reaction has an activation energy 10 kJ mol^{-1} higher than that of the but-2-enal reaction. The corresponding energy difference for model 2 is 19 kJ mol^{-1}. These results are in good agreement with the experimental measurements, which predict a energy difference of 14 kJ mol^{-1} on the basis of the more than two orders of magnitude higher reaction rate for but-2-enal than for 3-phenylprop-2-enal. Thus, our limited model systems are capable of reproducing the difference in reaction rate between the two substrates.

From the kinetic analysis, the activation free energy and activation enthalpy for the but-2-enal reaction in aqueous solution were computed to be 78 and 65 kJ mol^{-1}, respectively. These values are not directly comparable to the activation energy obtained by the DFT calculations, since the reference states are different. For the experimental data, the reference state is a loose substrate–enzyme complex (Michaelis complex), whereas the DFT calculations start from a reaction complex, a NAC. It should be noted that the MD simulations indicate that the free energy cost of going from the substrate–enzyme complex to the NAC (ΔG_{NAC}) is more than 9 kJ mol^{-1}. Furthermore, both the MD simulations and the kinetic study indicate that there is a very weak bonding of the aldehyde to the active site; that is, only a very loose enzyme–substrate complex is formed. The ΔG_{NAC} value would be expected to have a large entropic component, and it can be assumed that the change in enthalpy of going from the enzyme–substrate complex to the NAC is relatively small. Consequently, the experimentally determined activation enthalpy should be of a magnitude similar to that of the DFT-computed activation energy. There is also a relatively good agreement between the values; the computed activation energy for the large model system is 49 kJ mol^{-1}, which is only

16 kJ mol^{-1} lower than the experimentally measured activation enthalpy. This difference is within the accuracy of the DFT method, which for gas-phase chemical reactions is estimated to be around 16 kJ mol^{-1}.[32,33]

Conclusions

A new promiscuous activity of *C. antarctica* lipase B was used to catalyze the direct epoxidation of but-2-enal and 3-phenylprop-2-enal in aqueous and organic solution.

Substrate binding and binding of the reaction intermediate were investigated both by molecular dynamics (MD) simulations and by experimental kinetics. The MD simulations show that hydrogen peroxide binds tightly to His224 in both aqueous and acetonitrile solution. The aldehyde does not bind strongly to the oxyanion hole, and the binding is weaker in acetonitrile than in aqueous solution. This is in agreement with the kinetics, where no saturation was reached in acetonitrile and a relatively high K_M^{app} was determined in aqueous solution.

Density functional theory (DFT) computations indicate that the reaction proceeds through a two-step mechanism with formation of an oxyanionic intermediate. The first step, in which His224, with the support of Asp187, abstracts a proton from hydrogen peroxide in concert with the nucleophilic addition of hydrogen peroxide to the β-carbon, was found to be rate-determining. The second step, the ring closure, is catalyzed by the back-donation of the His224 proton to oxygen to form water. The MD and DFT results both indicate that oxyanion stabilization in transition states and intermediates are facilitated mainly by hydrogen bonds from Thr40. Hydrogen bonding from Gln106 was found to be less important. The experimental kinetic study is also indicative of the involvement of two hydrogen bonds in the transition state. The experimentally determined activation enthalpy is in relatively good agreement with the DFT calculations, in view of the different reference states and the accuracy of the DFT method. In addition, the difference in reaction rate between the but-2-enal and 3-phenylprop-2-enal is well reproduced by the DFT computations.

Experimental Section

Chemicals: But-2-enal and 3-phenylprop-2-enal (Fluka Chemika) were used as substrates. Hydrogen peroxide (35%, *w*/*w*) solution (SDS) was used as oxidant. Decane (Aldrich) and 1,4-dioxane (Labora) were used as internal standards for GC measurements. Acetonitrile (Labassco) was used as organic reaction solvent. KH_2PO_4 (Merck) buffer solution (100 mM), acidified to pH 3.9 with H_2PO_4 (Merck), was used as reaction solvent. Diethyl ether (VWR) and *n*-hexane (SDS) were used for the GC measurements.

Protein production: The *C. antarctica* lipase B Ser105Ala mutant was created by site-directed mutagenesis. Both wild-type and mutant lipases were expressed and produced in *Pichia pastoris,* purified by hydrophobic interaction chromatography and gel filtration, and freeze dried.[24,34]

Protein characterization: The amount of active enzyme was determined by active-site titration (with methyl *p*-nitrophenyl *n*-hexylphosphonate) of freeze-dried nonimmobilized wild-type CALB;[35] 78% of the enzyme was found to be active.[25]

Protein immobilization: Freeze-dried wild-type CALB and CALB Ser105Ala were immobilized on polypropylene carrier Accurel MP1000 (<1500 μm) in potassium phosphate buffer (50 mM, pH 8.6). Immobilized enzyme was dried and equilibrated to a water activity of 0.11. The amounts of protein adsorbed on the carrier were determined to 1.8% (*w*/*w*) for the wild-type lipase and 1.3% (*w*/*w*) for Ser105Ala mutant enzyme.[34,35]

Irreversible inhibition: Irreversible inhibition of immobilized wild-type CALB was carried out with methyl *p*-nitrophenyl *n*-hexylphosphonate as described by Rotticci et al.[35]

Direct epoxidation reactions: The typical direct epoxidation reaction mixture contained aldehyde (0.3 M), hydrogen peroxide (0.4 M, 35%, *w*/*w*), 1,4-dioxane or decane (0.3 M , internal standard), and solvent (100 mM KH_2PO_4 buffer of pH 3.9 or acetonitrile). Immobilized enzyme (12.5 mg, containing 1.8% (*w*/*w*) wild-type lipase or 1.3% (*w*/*w*) Ser105Ala mutant enzyme) was added to reaction solution (750 μL). The reactions were placed in an end-over-end rotator at 20 °C.

Compound quantities and identification: The quantitative analysis was carried out on a GC 5890 Series II (Hewlett Packard) instrument with FID detector and capillary column (CP-Chirasil Dex CB, 25 m × 0.32 mm i.d., d_f 0.25 μm). The temperature was set constant at 40 °C, and the retention times were: 4–4.5 min for but-2-enal, 5.5–6 min for the epoxide product, and 8 min for the 1,4-dioxane internal standard. Compound identification and characterization was carried out by using a GC-MS 6890 (Hewlett Packard) instrument with a capillary column (J&W CycloSil-B, 30 m × 0.32 mm i.d., d_f 0.25 μm) and fitted with an MS detector.

Enzyme kinetics: Enzyme kinetics for the direct epoxidation of but-2-enal catalyzed by wild-type CALB and Ser105Ala mutant were performed under pseudo-one-substrate conditions, the concentration of hydrogen peroxide being kept constant (0.4 M), while the concentration of but-2-enal was varied. 1,4-Dioxane or decane (0.3 M) were used as internal standards. Immobilized enzyme (12.5 mg, containing 1.8%, (*w*/*w*) wild-type CALB or 1.3% (*w*/*w*) CALB Ser105Ala) was added to the reaction volume of 750 μL. All reactions were performed at 20 °C in KH_2PO_4 buffer (pH 3.9, 100 mM) or acetonitrile. The concentrations of but-2-enal in acetonitrile were 0.003, 0.03, 0.3, 1 and 3 M, and those in water solution were 0.004, 0.009, 0.026, 0.14, 0.65 and 2.2 M. The kinetic constants—K_M^{app} and k_{cat}^{app}—and (k_{cat}/K_M^{app}) were determined from Hanes–Wolff plots by use of the apparent reaction rates and the substrate concentrations. The background reaction rates (k_{non}) were calculated from the equation: $v = k_{non}[S]_1[S]_2$, where $[S]_1$ and $[S]_2$ are the aldehyde and hydrogen peroxide concentrations. The initial background reaction rates were subtracted from the initial enzyme-catalyzed reaction rates.

Calculation of experimentally determined activation parameters: The initial rates of epoxidation of but-2-enal (0.3 M) by hydrogen peroxide (0.4 M) catalyzed by wild-type CALB and by CALB Ser105Ala, together with those of the uncatalyzed reaction, were determined at three or four constant temperatures: 15 °C, 30 °C, and 50 °C for reactions carried out in acetonitrile and 20, 30, 43, and 56 °C for those in water. The reaction mixture was prepared as described above. All mixtures were stirred to ensure even temperature diffusion. The thermodynamic activation components, Gibbs free energy ($\Delta G^{\neq}$), enthalpy ($\Delta H^{\neq}$), and entropy ($\Delta S^{\neq}$) were calculated from the Eyring equation.

Molecular dynamics simulations: Molecular dynamics simulations were performed for two sets of structures. The first involves hydrogen peroxide and 3-phenylprop-2-enal bound to the active site of CALB. This corresponds to the starting structure for the epoxidation of 3-phenylprop-2-enal. The second structure is an intermediate structure of the epoxidation reaction, where an oxygen of the hydrogen peroxide has bound to the β-carbon and the proton of the oxygen has transferred to His224. Starting structures for the MD simulations were generated from Autodock[36] simulations in which hydrogen peroxide, 3-phenylprop-2-enal, and the 3-phenylprop-2-enal epoxidation intermediate were docked to the 1LBT[20] crystal structure of CALB.

The AMBER9 package was used for all MD simulations, which were performed in acetonitrile and in aqueous solution.[37] The Amber 1999 force field (ff99) was used for the protein.[38] Force field parameters for the nonprotein atoms (belonging to hydrogen peroxide, 3-phenylprop-2-enal, and the intermediate structure formed from these) were generated by use of the antechamber program from the general Amber force field (gaff).[39,40] The generation of gaff-parameters was based on AM1 geometries, and the AM1-BCC approach was used for partial charges.[41,42] The TIP3P solvent model was used for water representation.[43] A united-atom model was used for the acetonitrile solvation.[44]

All amino acid residues were assumed to be in their natural protonation state, with the exception of His224, which was protonated in the simulations of the intermediate structure. The total charge was adjusted to zero by the addition of sodium counterions. Simulations were performed under periodic boundary conditions with a truncated octahedron unit cell, and the long-range electrostatics were handled by particle Mesh Ewald summation. A minimum layer of 8 Å solvent molecules were added outside the protein, which resulted in a unit cell that fitted a sphere of approximately 28 Å. The total numbers of atoms in the acetonitrile and aqueous solutions were approximately 12000 and 24000, respectively. Following initial minimization of 3500 steps in total, the systems were heated to 300 K over 20 ps with mild restraints on the protein atoms (10 kcal mol^{-1} Å). The production simulations were performed for 1 nanosecond with a time step of 2 fs and under constant temperature (300 K) and pressure (1.0 bar) conditions.

Density functional theory calculations: The reaction mechanism and the reaction energetics for the epoxidation in the Ser105Ala mutant of CALB were investigated by density functional theory (DFT) calculations. Two model systems were used to represent the reaction center in the active site (Figure 4). The first model includes fragments representing the amino acid residues Gln106, Thr40, His224, and Asp187. The second model omits Gln106, because the MD simulations indicated that this residue may not participate in the stabilization of transition states and reaction intermediates. The two different systems are referred to as model 1 and model 2, respectively throughout the text.

All stationary points, transition states and minima, have been fully optimized at the B3LYP/6–31 + G(d) level of theory. When hybrid-exchange correlation functionals, such as B3LYP, have been used, polarized valence double-ζ basis sets augmented with diffuse function have been shown to provide transition state barriers and reaction energetics of accuracy similar to that of much larger basis sets.[45] The positions of the catalytic residues were determined from the crystal structure of CALB (1LBT),[20] and a limited number (three for model 1 and two for model 2) of constraints were used to maintain the overall structure of the active site. The constraints ensured that the distance between His224 and Thr40, the distance between His224 and Gln106, and the distance between Thr40 and Gln106 were fixed. The specific atoms that were constrained are depicted in Figure 4. The reaction energies have been corrected for unspecific solvation effects by polarizable continuum model (PCM)[46] calculations at the B3LYP/6–31+G* level. A dielectric constant of 4.0 was assumed for the active site. The standard PCM method of Gaussian 03[47] was utilized; the solute cavities were made up of overlapping spheres centered at the nuclei. The radii of the spheres were taken as the Bondi[48] van der Waals radii and scaled by a factor of 1.2 (1.05 for polar hydrogens). The Gaussian 03 suite of programs was used for the DFT calculations.

Acknowledgements

This work was supported by the Swedish Research Council (VR), and by computing resources from the Swedish National Allocations Committee (SNAC).

Keywords: catalytic promiscuity · enzyme catalysis · epoxidation · hydrolases · molecular dynamics

[1] M. C. Capel-Sanchez, J. M. Campos-Martin, J. L. G. Fierro, M. P. de Frutos, A. Padilla Polo, *Chem. Commun.* **2000**, 855–856.
[2] C. C. Romão, F. E. Kühn, W. A. Herrmann, *Chem. Rev.* **1997**, *97*, 3197–3246.
[3] W. A. Herrmann, F. E. Kühn, *Acc. Chem. Res.* **1997**, *30*, 169–180.
[4] M. C. White, A. G. Doyle, E. N. Jacobsen, *J. Am. Chem. Soc.* **2001**, *123*, 7194–7195.
[5] F. G. Gelalcha, B. Bitterlich, G. Anilkumar, M. K. Tse, M. Beller, *Angew. Chem.* **2007**, *119*, 7266; *Angew. Chem. Int. Ed.* **2007**, *46*, 7293–7296.
[6] K.-H. Tong, K.-Y. Wong, T. H. Chan, *Tetrahedron* **2005**, *61*, 6009–6014.
[7] E. J. Allain, L. P. Hager, L. Deng, E. N. Jacobsen, *J. Am. Chem. Soc.* **1993**, *115*, 4415–4416.
[8] R. Furstoss, A. Archelas in *Enzyme Catalysis in Organic Synthesis, Vol. 2* (Eds.: K. Drauz, H. Waldmann), VCH, Weinheim, **1995**, pp. 694–695.
[9] P. Besse, H. Veschambre, *Tetrahedron* **1994**, *50*, 8885–8927.
[10] A. Zaks, D. R. Dodds, *J. Am. Chem. Soc.* **1995**, *117*, 10419–10424.
[11] F. Björkling, S. E. Godtfredsen, O. Kirk, *J. Chem. Soc. Chem. Commun.* **1990**, *19*, 1301–1303.
[12] F. Björkling, H. Frykman, S. E. Godtfredsen, O. Kirk, *Tetrahedron* **1992**, *48*, 4587–4592.
[13] S. Warwel, M. Rüsch gen. Klaas, *J. Mol. Catal. B Enzym.* **1995**, *1*, 29–35.
[14] R. Madeira Lau, F. van Rantwijk, K. R. Seddon, R. A. Sheldon, *Org. Lett.* **2000**, *2*, 4189–4191.
[15] V. M. Dembitsky, *Tetrahedron* **2003**, *59*, 4701–4720.
[16] V. Skouridou, H. Stamatis, F. N. Kolisis, *J. Mol. Catal. B* **2003**, *21*, 67–69.
[17] S. Bernasconi, F. Orsini, G. Sello, P. Di Gennaro, *Tetrahedron: Asymmetry* **2004**, *15*, 1603–1606.
[18] S. P. de Visser, F. Ogliaro, P. K. Sharma, S. Shaik, *J. Am. Chem. Soc.* **2002**, *124*, 11809–11826.
[19] G. Carrea, S. Colonna, D. R. Kelly, A. Lazcano, G. Ottolina, M. S. Roberts, *Trends Biotechnol.* **2005**, *23*, 507–513.
[20] J. Uppenberg, J. N. Ohrner, M. Norin, K. Hult, G. J. Kleywegt, S. Patkar, V. Waagen, T. Anthonsen, T. A. Jones, *Biochemistry* **1995**, *34*, 16838–16851.
[21] K. Hult, P. Berglund, *Trends Biotechnol.* **2007**, *25*, 231–238.
[22] M. D. Toscano, K. J. Woycechowsky, D. Hilvert, *Angew. Chem.* **2007**, *119*, 3274–3300; *Angew. Chem. Int. Ed.* **2007**, *46*, 3212–3236.
[23] P. Carlqvist, R. Eklund, K. Hult, T. Brinck, *J. Mol. Model.* **2003**, *9*, 164–171.
[24] C. Branneby, P. Carlvist, A. Magnusson, K. Hult, T. Brinck, P. Berglund, *J. Am. Chem. Soc.* **2003**, *125*, 874–875.
[25] C. Branneby, P. Carlvist, K. Hult, T. Brinck, P. Berglund, *J. Mol. Catal. B* **2004**, *31*, 123–128.
[26] P. Carlqvist, M. Svedendahl, C. Branneby, K. Hult, T. Brinck, P. Berglund, *ChemBioChem* **2005**, *6*, 331–336.
[27] M. Svedendahl, K. Hult, P. Berglund, *J. Am. Chem. Soc.* **2005**, *127*, 17988–17989.

[28] A. Magnusson, K. Hult, M. Holmquist, *J. Am. Chem. Soc.* **2001**, *123*, 4354–4355.
[29] F. A. Cotton, G. Wilkinson, P. L. Gaus, *Basic Inorganic Chemistry*, 2nd ed., Wiley, New York, **1987**.
[30] F. C. Lightstone, T. C. Bruice, *J. Am. Chem. Soc.* **1996**, *118*, 2595–2605.
[31] S. Hur, T. C. Bruice, *J. Am. Chem. Soc.* **2003**, *125*, 1472–1473.
[32] B. J. Lynch, D. G. Truhlar, *J. Phys. Chem. A* **2001**, *105*, 2936–2941.
[33] L. A. Curtiss, K. Raghavachari, P. C. Redfern, J. A. Pople, *J. Chem. Phys.* **2000**, *112*, 7374–7383.
[34] J. Rotticci-Mulder, M. Gustavsson, M. Holmqvist, K. Hult, M. Martinelle, *Protein Expression Purif.* **2001**, *21*, 386–392.
[35] D. Rotticci, T. Norin, K. Hult, M. Martinelle, *Biochim. Biophys. Acta Mol. Cell Biol. Lipids* **2000**, *1483*, 132–140.
[36] G. M. Morris, D. S. Goodsell, R. S. Halliday, R. Huey, W. E. Hart, R. K. Belew, A. J. Olson, *J. Comput. Chem.* **1998**, *19*, 1639–1662.
[37] D. A. Case, T. A. Darden, T. E. Cheatham III, C. L. Simmerling, J. Wang, R. E. Duke, R. Luo, K. M. Merz, D. A. Pearlman, M. Crowley, R. C. Walker, W. Zhang, B. Wang, S. Hayik, A. Roitberg, G. Seabra, K. F. Wong, F. Paesani, X. Wu, S. Brozell, V. Tsui, H. Gohlke, L. Yang, C. Tan, J. Mongan, V. Hornak, G. Cui, P. Beroza, D. H. Mathews, C. Schafmeister, W. S. Ross, P. A. Kollman, University of California, San Francisco, **2006**, AMBER 9.
[38] J. M. Wang, P. Cieplak, P. A. Kollman, *J. Comput. Chem.* **2000**, *21*, 1049–1074.
[39] J. M. Wang, W. Wang, P. A. Kollman, *Abstr. Pap. Am. Chem. Soc.* **2001**, *222*, U403–U403.
[40] J. M. Wang, R. M. Wolf, J. W. Caldwell, P. A. Kollman, D. A. Case, *J. Comput. Chem.* **2004**, *25*, 1157–1174.
[41] A. Jakalian, D. B. Jack, C. I. Bayly, *J. Comput. Chem.* **2002**, *23*, 1623–1641.
[42] A. Jakalian, B. L. Bush, D. B. Jack, C. I. Bayly, *J. Comput. Chem.* **2000**, *21*, 132–146.
[43] W. L. Jorgensen, J. Chandrasekhar, J. D. Madura, R. W. Impey, M. L. Klein, *J. Chem. Phys.* **1983**, *79*, 926–935.
[44] E. Guàrdia, R. Pinzón, J. Casulleras, M. Orozco, F. J. Luque, *Mol. Simulat.* **2001**, *26*, 287–306.
[45] B. J. Lynch, Y. Zhao, D. G. Truhlar, *J. Phys. Chem. A* **2003**, *107*, 1384–1388.
[46] J. Tomasi, M. Persico, *Chem. Rev.* **1994**, *94*, 2027–2094.
[47] M. J. Frisch, G. W. Trucks, H. B. Schlegel, G. E. Scuseria, M. A. Robb, J. R. Cheeseman, J. J. A. Montgomery, T. Vreven, K. N. Kudin, J. C. Burant, J. M. Millam, S. S. Iyengar, J. Tomasi, V. Barone, B. Mennucci, M. Cossi, G. Scalmani, N. Rega, G. A. Petersson, H. Nakatsuji, M. Hada, M. Ehara, K. Toyota, R. Fukuda, J. Hasegawa, M. Ishida, T. Nakajima, Y. Honda, O. Kitao, H. Nakai, M. Klene, X. Li, J. E. Knox, H. P. Hratchian, J. B. Cross, V. Backen, C. Adamo, J. Jaramillo, R. Gomperts, R. E. Stratmann, O. Yazyev, A. J. Austin, R. Cammi, C. Pomelli, J. W. Ochterski, P. Y. Ayala, K. Morokuma, G. A. Voth, P. Salvador, J. J. Dannenberg, V. G. Zakrzewski, S. Dapprich, A. D. Daniels, M. C. Strain, O. Farkas, D. K. Malick, A. D. Rabuck, K. Raghavachari, J. B. Foresman, J. V. Ortiz, Q. Cui, A. G. Baboul, S. Clifford, J. Cioslowski, B. B. Stefanov, G. Liu, A. Liashenko, P. Piskorz, I. Komaromi, R. L. Martin, D. J. Fox, T. Keith, M. A. Al-Laham, C. Y. Peng, A. Nanayakkara, M. Challacombe, P. M. W. Gill, B. Johnson, W. Chen, M. W. Wong, C. Gonzalez, J. A. Pople, Gaussian, Inc., Wallingford CT, **2004**, Gaussian 03 Revision C.02.
[48] A. Bondi, *Physical Properties of Molecular Crystals, Liquids and Glasses*, Wiley, New York, **1968**.

Received: May 9, 2008

